Nature Communications

https://doi.org/10.1038/s41467-026-70372-9

Article in Press

C6-ROMP Enabled by Structure-Guided Monomer Design for Chemically Recyclable Polymers

Received: 7 September 2025

Accepted: 24 February 2026

Cite this article as: Choi, K., Choi, W., Chung, M. *et al.* C6-ROMP Enabled by Structure-Guided Monomer Design for Chemically Recyclable Polymers. *Nat Commun* (2026). https://doi.org/10.1038/s41467-026-70372-9

Kyungmin Choi, Wootae Choi, Minjun Chung, Byeongwoo Im & Soon Hyeok Hong

C6-ROMP Enabled by Structure-Guided Monomer Design for Chemically Recyclable Polymers

Kyungmin Choi[1], Wootae Choi[1], Minjun Chung[1], Byeongwoo Im[1], and Soon Hyeok Hong[1]*

[1] Department of Chemistry, Korea Advanced Institute of Science and Technology (KAIST), Daejeon 34141, Republic of Korea

*Corresponding author email: soonhyeok.hong@kaist.ac.kr

Abstract: Cyclohexene, a minimally strained cyclic olefin, presents a long-standing challenge for ring-opening metathesis polymerization (ROMP) due to its inherently low ring strain energy. In this study, we present a rational monomer design framework for cyclohexene-derived monomers that leverages adaptive ring strain modulation via fused five-membered heterocycles—including carbonate, carbamate, acetal, silyl ether, and boronic ester motifs—to enhance polymerizability while enabling closed-loop recycling. Density functional theory (DFT) calculations and experimental thermodynamic analyses reveal how monomer conformation, ethenolysis ring strain energy (ERSE), and substituent effects govern ROMP thermodynamics and ring-closing metathesis depolymerization (RCMD) efficiency. An ERSE threshold of approximately 4.3 kcal/mol is identified as necessary for effective polymerization under mild conditions. Additionally, entropy differences driven by substituent flexibility significantly impact depolymerization temperature and efficiency. The resulting polymers exhibit tunable thermal properties, with glass transition temperatures ranging from −42 to 120 °C and efficient depolymerization performance. This study provides practical design principles for the development of sustainable functional polymers with predictable reactivity and recyclability.

Introduction

Polymers bearing a high density of functional groups—such as alcohols, amines, esters, acetals, boranes, or silanes—play vital roles in a wide range of applications due to the distinct chemical and physical properties conferred by these moieties.[1, 2, 3] By precisely tuning the nature and distribution of functional groups along the polymer backbone, key material attributes, including glass transition temperature, toughness, thermal stability, conductivity, and self-healing behavior, can be finely controlled, enabling the design of advanced functional materials.[4, 5]

Despite significant progress in functional polymer design,[6, 7] strategies that integrate broad functional group compatibility with chemical recyclability remain limited.[8, 9, 10, 11, 12, 13, 14] With growing demand for sustainable materials that combine enhanced performance with closed-loop lifecycles, there is a pressing need for recyclable polymer platforms capable of accommodating diverse functional architectures.[15, 16, 17, 18, 19, 20, 21]

Cyclohexene, the least-strained small cyclic olefin, has long posed a challenge in ring-opening metathesis polymerization (ROMP) due to its intrinsically low ring strain energy (RSE: 2.50 kcal/mol; ethenolysis ring strain energy, ERSE: 0.92 kcal/mol).[22, 23, 24, 25, 26, 27, 28] These values are significantly lower than those of other relatively less strained cyclic olefins such as cyclopentene (ERSE: 5.18 kcal/mol), cycloheptene (ERSE: 6.64 kcal/mol), and cyclooctene (ERSE: 8.21 kcal/mol). Consequently, cyclohexene derivatives have seen limited use in ROMP, typically requiring copolymerization with highly strained monomers[26, 27] or relying on cooperative mechanisms such as enyne metathesis.[23, 29] Early attempts, such as those by the McCarthy group, achieved only modest oligomerization (12% conversion, DP = 2–6) using $WCl_6/SnMe_4$ catalysts at −77 °C (Figure 1).[24] More recently, the Chen group reported a bridged γ–butyrolactone-cyclohexene monomer in which ring strain was enhanced through lactone bridging, enabling both ROMP and ring-opening polymerization (Figure 1).[25] However, such strategies inherently modify the six-membered ring structure, often introducing larger or more complex ring systems that compromise the native features of cyclohexene.

Nevertheless, cyclohexene derivatives remain attractive monomer candidates due to their facile synthesis from aromatic precursors, high potential for functionalization, and favorable depolymerization profiles via ring-closing metathesis,[10, 12, 30] enabled by their low RSE.[24, 28, 31, 32] Overcoming the challenge of polymerizability would unlock cyclohexene derivatives as a valuable platform for developing chemically recyclable functional polymers.

To address this challenge, we previously introduced a strategy based on adaptive ring strain modulation through reversible carbonate fusion.[22] In this system, trans-cyclic carbonate-fused cyclohexene monomers exhibited significantly increased ERSE (6.00 kcal/mol) due to conformational constraints, thereby enabling efficient ROMP. Subsequent deprotection yielded 1,2-diol-based polymers, which underwent efficient depolymerization under mild ring-closing metathesis depolymerization (RCMD) conditions, regenerating the low-RSE cyclohexene diols (ERSE = 1.93 kcal/mol). We questioned whether this strategy could be generalized to a wide range of functional groups, thereby enabling incorporation of diverse substituents into the polymer backbone to tailor material properties while controlling ERSE to facilitate both efficient ROMP and RCMD. Such an approach would provide a general platform

for densely functionalized yet chemically recyclable polymers, offering a compelling route toward next-generation materials that unite advanced functionality with closed-loop sustainability.

In the present study, we explore the generalizability of the adaptive ring strain modulation strategy by systematically introducing a diverse set of functional groups, including acetals (**TRAc/CRAc**), silyl ethers (**TRSil/CRSil**), carbonates (**TCbo**/**CCbo**), carbamates (**TRCbm**), and boronic esters (**TRBor**), into the fused cyclohexene scaffold (Figure 1). These functionalities not only modulate polymerization thermodynamics and the properties of the resulting polymers but also allow facile depolymerization by RCMD, either through direct ERSE control or by restoring the low-ERSE poly(cyclohexene-diol) backbone following deprotection. Through a combined theoretical and experimental analysis, we elucidate structure–thermodynamics relationships, focusing on how fused heterocycles and substituent effects influence molecular conformation, ring strain, and ROMP behavior.

Results

ERSE Calculations and Structure-ERSE Relationships

The ERSE of each monomer was calculated using density functional theory (DFT) at the B3LYP/6-31G(d,p) level of theory.[22] ERSE was defined by the following equation (1),[32] which represents the extent of enthalpic stabilization upon ring opening to serve as a predictor of monomer reactivity:

$$(1)\quad \mathrm{ERSE} = H_{\mathrm{monomer}} + H_{\mathrm{ethylene}} - H_{\mathrm{ring\text{-}opened}}$$

DFT calculations were performed on a series of cyclohexene-fused monomers bearing diverse functional groups—acetal, silyl ether, carbonate, carbamate, and boronic ester—selected for their known functional utility in polymer materials (Figure 1, Supplementary Table 3, Supplementary data 1). These variants were designed to assess how each functional group modulates ring strain via geometric distortion and conformational constraints. Generally, monomers undergo structural relaxation upon ring opening, primarily driven by the release of conformational strain. This stabilization occurs through bond rotation around the bridging C–C bond, allowing the fused-heterocycle and neighboring alkyl chains to adopt more favorable conformations. The conformational strain in the fused five-membered rings was investigated using Y–C–C–Y dihedral angles (θ, Y = O, N), specifically O–C–C–O or O–C–C–N, which reflect deviations before and after ring opening (Figure 2).

In their unfused forms, the calculated five-membered heterocycles adopt geometries characterized by Y–C–C–Y dihedral angles (θ) ranging from 0° to 34°, depending on ring flexibility and bonding characteristics (Figure 2). Among these calculated structures, boronic esters are the most planar, with a θ of just 0.02°. Carbonates, carbamates, and acetals adopt envelope conformations with modest dihedral angles (22.6°, 26.3°, and 26.4°, respectively). In contrast, silyl ethers adopt a half-chair conformation with the highest distortion in the series (θ = 34.3°), attributable to the longer Si–O bond length and greater angular flexibility.

Conversely, cyclohexene rings intrinsically favor a puckered, gauche-like conformation that minimizes torsional and steric strain. Around the C_4–C_5 bond, the adjacent bond dihedral angles vary depending on substituent orientation: H_{eq}–C_4–C_5–H_{eq} adopts a dihedral angle of 53°, while H_{eq}–C_4–C_5–H_{ax} reaches 63°, highlighting the non-planar, sterically relaxed nature of the cyclohexene framework (Figure 2).

This intrinsic geometric mismatch—between the near-planar geometry of five-membered heterocycles and the puckered conformation of cyclohexene—introduces conformational strain upon fusion. In trans-fused monomers, the heterocycle is connected to the equatorial positions of the cyclohexene ring, restricting the ability of the cyclohexene to adjust its conformation. Consequently, the heterocycle is forced into a more distorted geometry with an increased θ, contributing significantly to the overall ring strain and enhancing monomer reactivity.

Upon ring opening, this conformational constraint is relieved. The heterocycle relaxes toward its preferred geometry by reducing θ through bond rotation, as evidenced by consistently decreased dihedral angles in the ring-opened forms (blue angles in Figure 3 and 4). The magnitude of this geometric relaxation, expressed as $\Delta\theta = \theta_{cyclic} - \theta_{ring\text{-}opened}$, serves as a useful indicator of conformational strain release during polymerization.

In contrast, cis-fused monomers exhibit a different conformational behavior (Figure 2). While a geometric mismatch still exists when the cyclohexene adopts a half-chair conformation, the two C–Y bonds of the heterocycle are oriented on the same face of the ring system, enabling partial geometric accommodation. In this arrangement, the cyclohexene ring can adopt a slightly destabilized boat conformation, with a small dihedral angle of approximately 3° (H_{ax}–C_4–C_5–H_{ax}, boat). Meanwhile, heterocycles such as acetals, carbonates, and carbamates maintain near-planar geometries in the fused state (θ = 0.02–0.17°), with only modest energetic penalties (ΔG = 0.4–0.6 kcal/mol; see Supplementary Fig. 41, Supplementary Tables 4 and 5). This mutual adjustment between the cyclohexene and heterocycle enables the cis-fused ring system to achieve a more geometrically matched conformation, reducing conformational strain, θ values, and calculated heat of formation in the cyclic state.

However, upon ring opening, a new steric challenge emerges: both alkyl substituents are located on the same face of the ring-opened intermediate. Unlike trans-fused monomers, in which substituents naturally adopt a staggered or gauche arrangement, the cis configuration results in significant steric repulsion. This forces the heterocycle into additional distortion, increasing θ (red angles in Figure 3 and 4) and destabilizing the ring-opened form. As a result, cis-fused monomers typically exhibit lower ERSE values, reflecting reduced overall enthalpic stabilization upon ring opening.

Acetal Monomers

To provide a comparative reference for five-membered ring-fused cyclohexenes, we calculated the ERSE of a three-membered ring-fused monomer, *cis*-4,5-epoxy-1-cyclohexene (**45EP**). Due to the rigid and highly strained nature of the epoxide ring, its dihedral angle remains fixed at 0° in both cyclic and ring-opened forms (Figure 3). This rigidity prevents conformational stabilization upon ring opening; in fact, the ring-opened form becomes further destabilized by steric repulsion between the liberated alkyl chains, which adopt an eclipsed conformation. As a result, **45EP** exhibits a negative ERSE of –0.65 kcal/mol.

The behavior of cis-fused acetal monomers (**CdiMeAc**, **CnPrAc**, and **CPhAc,** Figure 3) resembles that of **45EP** in the cyclic state but diverges significantly upon ring opening due to the increased flexibility of the five-membered acetal ring. In the cyclic form, both C–O bonds in the acetal ring lie on the same face of the fused system, allowing the acetal ring to adopt a near-planar geometry ($\theta \approx 0°$), even as the cyclohexene ring assumes a boat conformation—similar to that observed in **45EP**. Upon ring opening, however, steric repulsion between the newly liberated alkyl chains becomes significant. Unlike the rigid epoxide, the acetal ring can accommodate this strain through conformational adjustment, distorting its C–O bond geometry to reduce eclipsing interactions. This structural change results in negative $\Delta\theta$ values. Although this introduces some conformational cost, partial energy recovery from the alleviated steric repulsion leads to moderately positive ERSE values (e.g., 1.15–1.94 kcal/mol for **CRAc**), though still lower than those of trans-fused analogs.

In contrast, trans-fused acetal monomers exhibit a clear trend of positive $\Delta\theta$, driven by the conformational mismatch between the cyclohexene and the fused heterocycle (Figure 2). In the cyclic form, the cyclohexene adopts a stable half-chair conformation, which forces the equatorially fused acetal ring into a distorted geometry with large dihedral angles (~40°, Figure 3). Upon ring opening, the acetal ring relaxes into a lower-energy envelope conformation with reduced dihedral angles, relieving conformational strain. This relaxation stabilizes the ring-opened form and is generally associated with higher ERSE values—for example, **TnPrAc** ($\Delta\theta = 16.8°$, ERSE = 4.30 kcal/mol) and **TPhAc** ($\Delta\theta = 22.3°$, ERSE = 4.44 kcal/mol).

DFT calculations further reveal that cis-fused isomers are thermodynamically more stable than their trans-fused counterparts. Specifically, **CnPrAc** is 1.43 kcal/mol more stable than **TnPrAc**, and **CPhAc** is 1.53 kcal/mol more stable than **TPhAc**, based on calculated free energies of formation. These results suggest that geometric compatibility between the heterocycle and the cyclohexene in cis-fused systems allows for mutual conformational accommodation, outweighing individual conformational preferences and leading to overall thermodynamic stabilization.

Silyl Ether Monomers

Silyl ether monomers, in contrast to other heterocycles, display limited conformational distortion and strain modulation in both trans- and cis-fused configurations (Figure 3). Presumably owing to the longer Si–O bond length and inherent geometric flexibility, silyl ethers adopt a C_5 half-chair conformation in both cyclic and ring-opened forms. In the unfused state, the five-membered silyl ether ring already exhibits relatively large O–C–C–O dihedral angles—34.3° for the dimethyl variant and 30.8° for the tert-butyl analog—which limits the extent of additional ring strain introduced upon trans-fusion to cyclohexene.

As a result, **TdiMeSil** and **TditBuSil** exhibit modest conformational changes upon ring opening, with $\Delta\theta$ values of 11.0° and 10.2°, and correspondingly low ERSEs of 2.56 and 2.78 kcal/mol, respectively. The similarity in both $\Delta\theta$ and ERSE between these monomers suggests that the nature of the substituent on silicon (Me vs tBu) has minimal influence on the overall ring strain and conformational dynamics in trans-fused systems.

In contrast, cis-fused silyl ether monomers exhibit greater sensitivity to substituent effects, which affect their C_5-ring conformation. In **CdiMeSil**, the half-chair geometry is retained in both the cyclic and ring-opened forms due to its inherently large θ, resulting in a modest Δθ of 5.6° and a ERSE of 2.04 kcal/mol. However, in **CditBuSil**, the bulky tert-butyl group introduces steric repulsion with the axial proton on the cyclohexene ring. This interaction distorts the heterocycle into a more planar, envelope-like geometry, resulting in a negative Δθ of –20.1° and a markedly lower ERSE of 0.67 kcal/mol, indicating less stabilization upon ring opening like other planar cis-fused heterocycles.

Overall, both acetal and silyl ether monomers, which feature cyclopentane-like fused-ring topologies, exhibit limited conformational stabilization upon ring opening, owing to the relatively small energy differences between accessible conformers. Consequently, their ERSE values remain low, reflecting only modest enthalpic gains from strain relief during polymerization.[33]

Carbonate and Carbamate Monomers

Carbonate and carbamate monomers, both containing carbonyl groups capable of π-conjugation, exhibit more pronounced ring strain associated with conformational change than cyclopentene-like fused-ring systems (Figure 4). The carbonate-protected monomers show pronounced differences between their trans- and cis-fused isomers. **TCbo** (trans) exhibits a Δθ of 14.3° and an ERSE of 6.00 kcal/mol, while **CCbo** (cis) shows a negative Δθ of –26.5° and a much lower ERSE of 0.91 kcal/mol.

TCbo follows the expected behavior of trans-fused monomers. In its cyclic form, the C–O bonds are oriented in opposite directions, introducing conformational strain that is relieved upon ring opening. This strain release leads to a significant ERSE. In contrast, **CCbo** aligns both C–O bonds on the same side, minimizing strain in the cyclic state (θ = 0.02°). However, upon ring opening, steric repulsion between the liberated alkyl chains increases, raising the dihedral angle and resulting in only modest stabilization (Δθ = –26.5°; ERSE = 0.91 kcal/mol). DFT calculations further reveal that **CCbo** is 3.34 kcal/mol more stable than **TCbo** in terms of heat of formation, again emphasizing the effect of geometric compatibility.

Carbamate monomers exhibit similar trends, with Δθ values ranging from 6.6° to 15.7° and ERSE values from 4.25 to 5.54 kcal/mol. Both carbonate and carbamate monomers display higher ERSEs than acetal and silyl ether monomers with similar or smaller Δθ values, which can be attributed to the increased rigidity of their carbonyl-containing fused rings. This rigidity resists conformational distortion, leading to a greater enthalpic difference between cyclic and ring-opened forms, and thus greater ring strain upon polymerization.

In addition to ring rigidity, carbamate monomers demonstrate clear substituent effects on ERSE, driven by steric interactions at the nitrogen center (Figure 5). For instance, **TtBuCbm** shows the second-highest ERSE (5.25 kcal/mol) among the carbamates, likely due to substantial steric repulsion between the bulky tert-butyl group and the cyclohexene ring, which destabilizes the cyclic form. In contrast, **TiPrCbm**, bearing a less hindered isopropyl group, exhibits a lower ERSE of 4.25 kcal/mol, consistent with reduced steric strain.

To quantify these effects, the distance between the nitrogen substituent and the allylic carbon of the cyclohexene ring was measured across the series. Upon ring opening, this distance increased by 0.197 Å (**TAcCbm**), 0.099 Å (**TPhCbm**), and 0.374 Å (**TtBuCbm**), indicating steric relief. In contrast, **TiPrCbm** showed a slight decrease (–0.038 Å), suggesting a different steric profile and reduced conformational reorganization.

In cyclic forms with bulky substituents such as Ac, Ph, and tBu, close proximity to the cyclohexene ring leads to destabilization. Upon ring opening, the adjacent alkyl chain rotates away from the substituent, alleviating steric repulsion and increasing the energy gap between cyclic and ring-opened states—thus raising ERSE. Conversely, in **TiPrCbm**, the less hindered hydrogen on the isopropyl group faces the cyclohexene ring, minimizing repulsion in the cyclic state. After ring opening, the chain reorients slightly toward the substituent to relieve steric conflict with the neighboring alkyl chain. This limited rearrangement results in a correspondingly lower ERSE.

Boronic Ester Monomers

Finally, boronic ester monomers exhibit a distinct influence of ring flexibility on ERSE behavior (Figure 4). Unlike the more rigid carbonate and carbamate rings, boronic esters are conformationally adaptable due to the empty p orbital on boron, which facilitates bond angle distortion and relieves strain upon fusion.[34, 35, 36] Optimized geometries of **TPhBor** and **TnBuBor** reveal substantial deviations from planarity, with Δθ values of 21.4° and 27.0°, respectively—significantly higher than that of **TCbo** (Δθ = 14.3°).

However, despite their larger Δθ values, both boronic ester monomers display comparable ERSEs (~6.0 kcal/mol), which do not increase significantly with angular distortion. This observation suggests that the flexible boronic ester ring accommodates dihedral changes with minimal energetic penalty. In contrast to rigid carbonyl-based systems, where ring distortion leads to a significant increase in ring strain, the inherent flexibility of boronic esters allows substantial geometric adjustment without a corresponding rise in ERSE. These findings highlight the role of ring rigidity—rather than angular distortion alone—in modulating ring strain and reactivity in fused cyclic systems.

Thermodynamics Study of Various Fused-Ring Cyclohexene Monomers

Building on the theoretical insights from ERSE calculations, we conducted a detailed thermodynamic analysis of the polymerization behavior of various fused-ring cyclohexene monomers (Figure 6). Specifically, we examined the relationship between experimentally measured polymerization enthalpy (ΔH_p), entropy (ΔS_p), and their correlation with calculated ERSE values. The ΔH_p and ΔS_p values were determined from van't Hoff plot generated using polymerization data collected across a range of temperatures. All polymerizations were carried out under standard conditions (2.0 M CH_2Cl_2, 0.50 mol% of **G3**).

To facilitate more direct comparison with other polymer systems, ceiling temperatures (T_c) were measured under 1.0 M CH_2Cl_2 conditions, except in the case of **TiPrCbm**, which only underwent polymerization at 2.0 M (Figure 6, Supplementary Table 1). The experimentally measured ΔH_p (2.0 M) values for the monomers ranged from –3.92

kcal/mol to –1.59 kcal/mol, while ΔS_p (2.0 M) values ranged from –12.4 to –1.21 cal/mol·K. These thermodynamic parameters led to a broad range of T_c (1.0 M) values, spanning from 0 to 550 °C.

Entropy Change for Polymerization (ΔS_p)

The variation in ΔS_p across monomers is primarily governed by the nature of the fused-ring heterocycles and the substituent structures. Generally, monomers bearing substituents with limited conformational freedom tend to exhibit larger decreases in ΔS_p. (Figure 7, Supplementary Table 1) The overall entropy change during the polymerization arises from two primary contributions: (1) the translational entropy loss due to a reduction in the number of molecules and (2) the rotational entropy and structural entropy change associated with converting a cyclic monomer into a linear, ring-opened repeat unit.[37] Since the translational contribution is consistent across monomers, the dominant source of ΔS_p variability lie in differences in rotational and vibrational freedom between the monomer and the corresponding polymer chain segment.

In cyclic monomers, the influence of side-chain substituent is limited because the constrained ring framework restricts meaningful interactions between the substituent and the cyclohexene core. Upon ring opening, the monomer becomes a part of a flexible polymer chain, enabling greater interaction between side-chain substituent and linear backbone. The transition amplifies the effect of substituent structure, interchain interactions, and ring-flexibility on the accessible conformational landscape of the polymer. Symmetric, bulky, or rigid substituents restrict local segmental motion and reduce the entropy gain, whereas flexible or asymmetric groups preserve greater conformational freedom and mitigate entropy loss.

Among the carbonyl-containing monomers, **TCbo** exhibits a moderate ΔS_p of –8.16 cal/mol·K. The carbamate monomers **TPhCbm** (–7.90 cal/mol·K) and **TAcCbm** (–8.68 cal/mol·K) show similar entropy losses, likely due to their rigid π-conjugated substituents, which restrict rotational freedom in the polymer state (Figure 7). In contrast, **TiPrCbm** displays a significantly less negative ΔS_p (–6.77 cal/mol·K), attributable to the asymmetric and flexible isopropyl group, which increases the number of distinguishable orientations and enhances segmental mobility, thereby reducing the overall entropy loss.

On the other hand, **TtBuCbm** exhibits a substantial entropy decrease (–11.3 cal/mol·K). The tert-butyl group's high symmetry reduces its conformational entropy in the polymer, and its bulkiness further limits segmental motion, both of which contribute to a large net entropy loss during polymerization.

Acetal monomers, which feature sp^3-hybridized ring centers, also show clear substituent effects. **TnPrAc** exhibits a moderate ΔS_p of –7.64 cal/mol·K, while **TPhAc** records the highest entropy loss among the fused-ring series at –12.4 cal/mol·K. This contrast can be explained by the greater flexibility of the n-propyl group compared to the more rigid and planar phenyl group, which suppresses conformational degrees of freedom.

Interestingly, the acetal monomers display a pronounced concentration-dependent behavior. At 1.0 M, their ΔS_p values are notably reduced—**TnPrAc** decreases to –3.19 cal/mol·K and **TPhAc** to –6.07 cal/mol·K—making them substantially lower than most of the other monomers, whereas the remaining monomer series shows only modest

variation. This behavior may arise in part from the substituent interactions or the envelope conformation adopted by the acetal ring during ring opening: the alignment of both C–O bonds in the same direction increases the dipole moment of the repeat unit, in contrast to other monomers whose C–Y bonds are oriented oppositely. At higher concentrations, enhanced intermolecular interactions may further stabilize the ring-opened state and reduce conformational freedom, contributing to the observed increase in entropy loss.

Finally, the boronic ester monomers **TPhBor** (–5.48 cal/mol·K) and **TnBuBor** (–1.21 cal/mol·K) exhibit the smallest entropy changes among the series. This can be attributed to the inherent flexibility of the boronic ester ring, which permits a broader conformational ensemble in both monomer and polymer states. As a result, the polymer backbone retains substantial segmental freedom, particularly in the motion of appended alkyl chains in backbone. Substituent effects further modulate this behavior: **TnBuBor**'s lower ΔS_p relative to **TPhBor** likely reflects the greater flexibility and segmental mobility of the *n*-butyl group compared to the more rigid phenyl substituent.

ERSE-Polymerization Thermodynamics Relationships

To assess the thermodynamic driving force for ROMP, we investigated the relationship between polymerization enthalpy (ΔH_p) and DFT-calculated ERSE across various fused-ring cyclohexene monomers (Figure 8a, 8b, Supplementary Table 1). In general, experimentally measured ΔH_p values were lower than the corresponding ERSE values. This disparity arises from the differences in model assumptions: ERSE is based on idealized ethenolysis reactions involving ethylene and terminal olefins, whereas ΔH_p reflects the average enthalpic release during actual polymerization, including steric contributions from adjacent monomer units in growing polymer chains and Ru-based alkylidene catalysts at each chain end, and possible energy absorbed by the polymer conformation.[38] Additionally, ΔH_p encompasses potential side reactions, such as secondary metathesis and macrocyclic oligomer formation. Nevertheless, as monomer ring strain remains the dominant factor, ΔH_p trends correlate with ERSE.

Comparative analysis revealed a generally linear correlation between ΔH_p and ERSE across the set of polymerizable monomers. Although a strict linear relationship is obscured by secondary structural factors (e.g. interchain stacking, conformational flexibility, and substituent effects), ERSE remains a reliable predictor of the thermodynamic feasibility of polymerization. At 2.0 M, the ROMP threshold emerged between ERSE values of 2.78 and 4.25 kcal/mol. Monomers below this range, including **45EP**, **CCbo**, **CdiMeAc**, **TdiMeSil**, and **TditBuSil**, failed to polymerize above –30 °C, indicating insufficient ring strain to drive the reaction. At 1.0 M, this threshold shifted higher due to increased entropy loss at lower concentrations, reinforcing 4.25 kcal/mol as the effective minimum ERSE for ROMP under ambient or mild conditions.

While the ERSE-ΔH_p relationship captures the behavior of most monomers, notable deviations were analyzed to elucidate the influence of secondary structural effects. In particular, **TPhAc** (ERSE = 4.30 kcal/mol) exhibited a significantly more exothermic ΔH_p at 2.0 M (–3.52 kcal/mol) than predicted. One possible explanation is that this stabilization in the polymer state can be attributed to enhanced interchain π–π stacking or dipole interactions. DFT calculations reveal that the phenyl group in **TPhAc** rotates ~90° upon ring opening, adopting a perpendicular

orientation relative to the acetal ring. This conformational shift, along with the increased dipole moment of the ring-opened structure, could facilitate interchain stacking and contributes to a more favorable ΔH_p than ERSE alone would suggest.

This concentration-dependent stabilization was further suggested by ΔH_p measurements at 1.0 M, where **TPhAc**'s ΔH_p decreased to –1.84 kcal/mol ($\Delta(\Delta H_p)$ = 1.68 kcal/mol), aligning more closely with the ERSE–ΔH_p trend. A similar, though less pronounced, effect was observed for **TnPrAc**, with ΔH_p shifting from –2.08 kcal/mol at 2.0 M to –1.00 kcal/mol at 1.0 M ($\Delta(\Delta H_p)$ = 1.08 kcal/mol). These observations are consistent with the possibility that acetal-specific interchain interactions, such as dipole alignment, and the effect of π–π stacking, may affect chain conformation and help stabilize the polymer under concentrated conditions.[38]

To deepen our understanding of these concentration effects on thermodynamics of acetal monomers, we expanded the study to include intermediate and higher concentrations (1.5 M, 2.5 M, and, for **TnPrAc**, 3.0 M, Supplementary Table 1). These additional measurements revealed that **TPhAc** exhibits two distinct regimes (Figure 8c): from 1.0 M to 2.0 M, both ΔH_p and ΔS_p become increasingly negative, consistent with progressively stronger π–π stacking and acetal packing; however, at 2.5 M, ΔH_p plateaus while ΔS_p becomes slightly less negative, indicating saturation of stabilizing interactions coupled with reduced translational entropy in the monomer state. In contrast, **TnPrAc**, lacking aromatic π-stacking, does not show a saturation plateau in ΔH_p (Figure 8d); instead, its enthalpy becomes steadily more exothermic up to 3.0 M, reflecting gradual enhancement of van der Waals–driven packing of its flexible *n*-propyl substituent. ΔS_p for **TnPrAc** reaches a minimum at 2.0 M and then remains relatively constant through 3.0 M, consistent with a more conventional, less cooperative packing process. These extended measurements reinforce that the strong concentration dependence observed in acetal monomers originates from the distinct packing modes and substituent-specific interactions in their ring-opened polymer structures.

In contrast, boronic ester monomers (**TnBuBor**, **TPhBor**) consistently exhibited lower ΔH_p values than expected from their ERSEs. This deviation is likely due to the high conformational flexibility of boronic ester rings. While ERSE calculations are based on the enthalpy difference between the lowest-energy conformers of cyclic and ring-opened forms, experimental ΔH_p reflects an ensemble average over all accessible conformations during polymerization.[39] Upon ring opening, the boronic ester units introduce substantial rotational freedom, allowing access to higher-energy conformers. This increases the average energy of the ring-opened state, effectively lowering the observed enthalpic driving force.

Additional deviations in ΔH_p were observed in monomers bearing long, flexible alkyl substituents such as **TnPrAc** and **TnBuBor**. Despite having relatively higher ERSE values than their phenyl-substituted analogs (**TPhAc** and **TPhBor**), these monomers exhibited lower ΔH_p values. This suggests that steric clashes between the long-chain alkyl substituents and the propagating polymer chain or the bulky Ru alkylidene moiety at the chain ends may destabilize the ring-opened intermediate. Such steric effects are not captured in ERSE calculations, but may play a significant role in real polymerization environments.

Taken together, these findings indicate that while ERSE serves as a reliable baseline metric for predicting monomer reactivity, accurate thermodynamic modeling of ROMP must also consider interchain interactions, backbone flexibility, and remote substituent effects. From these trends, practical thresholds emerge:

- **ERSE < 2.8 kcal/mol**: Monomers are generally non-polymerizable under standard conditions.
- **ERSE ≥ 4.3 kcal/mol**: Monomers reliably polymerize, defining the effective minimum threshold.
- **ERSE > 5.0 kcal/mol**: Preferred for efficient polymerization under mild conditions (e.g., CH_2Cl_2, 2.0 M, r.t.).

These design rules validate ERSE as a useful screening tool for monomer development, while also highlighting additional structural features that modulate polymerization efficiency.

Depolymerization Study

The established thermodynamic profiles were directly reflected in the RCMD behavior of the polymers. Although the variation in polymerization enthalpy (ΔH_p) across monomers was relatively small, substantial differences in polymerization entropy (ΔS_p) produced a wide range of ceiling temperatures ($T_c = \Delta H_p/\Delta S_p$), leading to markedly different depolymerization behaviors. Depolymerization reactions were systematically screened over a range of concentrations and temperatures (Supplementary Table 2). In conventional RCMD processes, high depolymerization efficiencies are typically achieved only under highly dilute conditions (<0.1 M),[25, 30, 40] requiring large solvent volumes. By utilizing cyclohexene monomers and tuning their polymerization thermodynamics, we identified conditions that enable excellent depolymerization efficiency (>90%) at comparatively higher concentrations. Accordingly, Table 1 reports the highest concentration conditions that maintain excellent depolymerization efficiency, highlighting the practical advantage of this thermodynamic design strategy of cyclohexene.

A wide range of T_c values from 0 to 550 °C was obtained by controlling the substituent on monomers affecting ΔH_p and ΔS_p values. Importantly, polymers with T_c below 100 °C showed excellent RCMD efficiency under mild thermal conditions and at relatively high concentrations (≥200 mM at 40 °C). For example, **PTiPrCbm**, **PTPhAc**, and **PTnPrAc** exhibited quantitative monomer recovery (>96%) under these conditions. Notably, **PTAcCbm**, with a moderately higher T_c (118.1 °C), also demonstrated excellent RCMD efficiency under mild conditions (40 °C, 100 mM).

In contrast, polymers with T_c values above 200 °C, such as **PTCbo**, **PTPhBor**, and **PTnBuBor**, showed poor depolymerization efficiency. Under standard RCMD conditions (40–60 °C, 100 mM), these high-T_c polymers yielded less than 60% monomer recovery.

Despite this variability, all diol-based polymers synthesized in this study can be quantitatively deprotected via hydrolysis to yield poly(cyclohexene-4,5-diol) (**PC6diol**)—a previously reported material that undergoes highly efficient RCMD at 25 °C and 320 mM with quantitative monomer recovery.[22] These substituent-controlled low T_c

polymers and two-stage degradation strategies (deprotection followed by RCMD) offers a robust route to chemical recycling for high-performance materials that otherwise resist depolymerization under mild conditions.

Polymer Properties

The molecular weight and thermal properties of the resulting polymers are summarized in Figure 9 (see also Supplementary Fig. 33–40). Polymerizations were performed in dichloromethane at an initial monomer concentration of 2.0 M using monomer-to-initiator ratios of 200:1, 300:1, 500:1, and 1000:1. All polymerizations showed controlled molecular weight growth, with linear increases in number-average molecular weight (M_n) proportional to the effective degree of polymerization (Supplementary Fig. 14–22), indicative of controlled ROMP behavior.

High-molecular-weight polymers (>50 kDa) were obtained for most monomers at a 1000:1 monomer-to-initiator ratio. Thermal analysis revealed that all polymers exhibited high thermal stability, with decomposition temperatures (T_d) exceeding 200 °C, except for **PTPhAc**. The glass transition temperatures (T_g) ranged widely from –42 °C to 120 °C, underscoring the tunable thermal properties enabled by the fused-ring cyclohexene architecture.

T_g values were strongly influenced by the nature and position of the substituents. **PTCbo**, which lacks substituents, served as a reference with a T_g of 65 °C. Carbamate-based polymers bearing nitrogen-bound substituents adjacent to the polymer backbone exhibited elevated T_g values relative to **PTCbo**. This trend is attributed to increased steric hindrance near the backbone, which restricts segmental motion and increases chain rigidity, thereby raising T_g. Consistent with this rationale, T_g increased with substituent bulk: from **PTCbo**, followed by **PTiPrCbm**, **PTPhCbm**, **PTAcCbm**, and **PTtBuCbm**, featuring the most sterically demanding *tert*-butyl group, exhibited the highest T_g at 120 °C.

In contrast, substituents located farther from the backbone, located on the central atom of the fused ring, as in **PTRAc** and **PTRBor** polymers, exert the opposite effect. These polymers generally displayed lower T_g values (below 55 °C). The reduced T_g is attributed to less efficient chain packing in the solid state: bulky or flexible substituents remote from the backbone introduce additional free volume and enhance chain mobility. Consistent with this interpretation, **PTPhBor** and **PTPhAc** shows decreased T_g compared to **PTCbo** and **PTPhCbm**. This effect became more pronounced with longer and more flexible aliphatic substituents, as seen in **PTnPrAc** and **PTnBuBor**, which showed the lowest T_g values of –29 °C and –42 °C, respectively. These observations demonstrate how substituent position, steric environment, and packing efficiency influence the thermomechanical behavior and enable tuning of polymer thermal properties through monomer design.

Discussion

This study establishes a general and versatile strategy for designing ROMP-based chemically recyclable polymers via adaptive ring strain modulation of cyclohexene derivatives. By systematically varying fused

heterocycles and substituents, we elucidated how subtle conformational and steric features influence polymerization and depolymerization thermodynamics. Our integrated computational and experimental approach revealed that while ERSE provides a reliable predictive metric for monomer reactivity, additional factors—such as fused-ring flexibility, interchain interactions, and remote substituent effects—should be considered for thermodynamic profiling under practical polymerization conditions.

We identified a critical ERSE threshold (~4.25 kcal/mol) necessary for efficient ROMP under mild conditions, providing a valuable design guideline for future monomer development. Moreover, polymerization entropy (ΔS_p) was shown to be independently tunable by substituent structure and concentration, directly impacting depolymerization efficiency via modulation of ceiling temperature (T_c). This thermodynamic control enables fine-tuning of closed-loop recyclability and expands the operational window for RCMD.

Beyond reactivity, we demonstrated that thermomechanical properties—particularly glass transition temperatures (T_g)—can be precisely modulated by the position and nature of substituents. Substituents near the polymer backbone increased T_g via restricted segmental mobility, while remote or flexible substituents decreased T_g by enhancing chain mobility and disrupting packing.

Altogether, this work provides a blueprint for the rational design of fused-ring cyclohexene monomers that combine chemical recyclability with tunable physical properties. The insights presented here advance the molecular-level understanding of ROMP thermodynamics and lay the foundation for developing next-generation sustainable polymers with tailored functionality for broad application.

Methods

General procedure for ROMP

In a vial, monomer (200-1000 eq.) was added. The initiator stock solution (20 μL,1 eq.) was prepared with anhydrous CH_2Cl_2. The monomer solution was prepared to achieve the desired monomer concentration (2.0 M) after adding initiator solution. The reaction was equilibrated at set temperature for 5 min, then the initiator solution was added. Upon completion, the reaction was quenched with excess ethyl vinyl ether (0.10 mL). The volatiles were removed, and the crude mixture was analyzed by ^{1}H NMR, and conversion was determined through comparison of olefin C–H signals. The polymer was purified by repeated precipitation in methanol.

General procedure for RCMD

In a stirring-bar charged reaction vial, polymer (0.28 mmol), **G2** catalyst (0.0028 mmol, 1.0 mol%), and CH_2Cl_2 (0.10 or 0.20 M concentration to olefin) were added in inert condition. The reaction was stirred 12 h. The reaction was quenched with the addition of excess ethyl vinyl ether. The crude mixture was analyzed by ^{1}H NMR, conversion was calculated by comparing the olefin signals.

Data availability

Detailed experimental procedures, computational details, characterization data are available from the Supplementary Information. The Cartesian Coordinates of the calculated structures are available from the Supplementary Data 1. All data are available from the corresponding author upon request.

References

1. Franssen, N. M., Reek, J. N. & de Bruin, B. Synthesis of functional 'polyolefins': State of the art and remaining challenges. *Chem. Soc. Rev.* **42**, 5809-5832 (2013).

2. Rodriguez, G. M., Díaz-Requejo, M. M. & Pérez, P. J. Metal-catalyzed postpolymerization strategies for polar group incorporation into polyolefins containing C–C, C═C, and aromatic rings. *Macromolecules* **54**, 4971-4985 (2021).

3. Varghese, A. M. & Karanikolos, G. N. CO_2 capture adsorbents functionalized by amine – bearing polymers: a review. *Int. J. Greenh. Gas Control* **96**, 103005 (2020).

4. Boaen, N. K. & Hillmyer, M. A. Post-polymerization functionalization of polyolefins. *Chem. Soc. Rev.* **34**, 267-275 (2005).

5. Wang, K. et al. Advanced functional polymer materials. *Mater. Chem. Front.* **4**, 1803-1915 (2020).

6. Kobayashi, S., Pitet, L. M. & Hillmyer, M. A. Regio- and stereoselective ring-opening metathesis polymerization of 3-substituted cyclooctenes. *J. Am. Chem. Soc.* **133**, 5794-5797 (2011).

7. Dingwell, C. E. & Hillmyer, M. A. Regiospecific poly(ethylene-co-vinyl alcohol) by ROMP of 3-acetoxycyclooctene and postpolymerization modification for barrier material applications. *ACS Appl. Polym. Mater.* **5**, 1828-1836 (2023).

8. Shieh, P., Nguyen, H. V. & Johnson, J. A. Tailored silyl ether monomers enable backbone-degradable polynorbornene-based linear, bottlebrush and star copolymers through ROMP. *Nat. Chem.* **11**, 1124-1132 (2019).

9. Shieh, P. et al. Cleavable comonomers enable degradable, recyclable thermoset plastics. *Nature* **583**, 542-547 (2020).

10. Feist, J. D. & Xia, Y. Enol ethers are effective monomers for ring-opening metathesis polymerization: synthesis of degradable and depolymerizable poly(2,3-dihydrofuran). *J. Am. Chem. Soc.* **142**, 1186-1189 (2020).

11. Feist, J. D., Lee, D. C. & Xia, Y. A versatile approach for the synthesis of degradable polymers via controlled ring-opening metathesis copolymerization. *Nat. Chem.* **14**, 53-58 (2022).

12. Sathe, D. et al. Olefin metathesis-based chemically recyclable polymers enabled by fused-ring monomers. *Nat. Chem.* **13**, 743-750 (2021).

13. Fraser, C., Hillmyer, M. A., Gutierrez, E. & Grubbs, R. H. Degradable cyclooctadiene/acetal copolymers: versatile precursors to 1,4-hydroxytelechelic polybutadiene and hydroxytelechelic polyethylene. *Macromolecules* **28**, 7256-7261 (1995).

14. Pal, A., Wong, A. R. & Lamb, J. R. Chemically recyclable, high molar mass polyoxazolidinones via ring-opening metathesis polymerization. *ACS Macro Lett.* **13**, 502-507 (2024).

15. Plummer, C. M., Li, L. & Chen, Y. Ring-opening polymerization for the goal of chemically recyclable polymers. *Macromolecules* **56**, 731-750 (2023).

16. Jehanno, C. et al. Critical advances and future opportunities in upcycling commodity polymers. *Nature* **603**, 803-814 (2022).

17. Shi, C. et al. Design principles for intrinsically circular polymers with tunable properties. *Chem* **7**, 2896-2912 (2021).

18. Purohit, V. B., Pięta, M., Pietrasik, J. & Plummer, C. M. Towards sustainability and a circular economy: ROMP for the goal of fully degradable and chemically recyclable polymers. *Eur. Polym. J.* **208**, 112847 (2024).

19. Ibrahim, T. et al. Chemical recycling of polyolefins via ring-closing metathesis depolymerization. *Chem. Commun.* **60**, 1361-1371 (2024).

20. Kim, S. & Chung, H. Biodegradable polymers: from synthesis methods to applications of lignin-graft-polyester. *Green Chem.* **26**, 10774-10803 (2024).

21. Zhou, J., Sathe, D. & Wang, J. Understanding the structure-polymerization thermodynamics relationships of fused-ring cyclooctenes for developing chemically recyclable polymers. *J. Am. Chem. Soc.* **144**, 928-934 (2022).

22. Choi, K. & Hong, S. H. Chemically recyclable oxygen-protective polymers developed by ring-opening metathesis homopolymerization of cyclohexene derivatives. *Chem* **9**, 2637-2654 (2023).

23. Park, H. & Choi, T.-L. Fast tandem ring-opening/ring-closing metathesis polymerization from a monomer containing cyclohexene and terminal alkyne. *J. Am. Chem. Soc.* **134**, 7270-7273 (2012).

24. Patton, P. A., Lillya, C. P. & McCarthy, T. J. Olefin metathesis of cyclohexene. *Macromolecules* **19**, 1266-1268 (2002).

25. Shi, C., Clarke, R. W., McGraw, M. L. & Chen, E. Y. Closing the "one monomer-two polymers-one monomer" loop via orthogonal (de)polymerization of a lactone/olefin hybrid. *J. Am. Chem. Soc.* **144**, 2264-2275 (2022).

26. Song, A., Parker, K. A. & Sampson, N. S. Synthesis of copolymers by alternating ROMP (AROMP). *J. Am. Chem. Soc.* **131**, 3444-3445 (2009).

27. Song, A., Parker, K. A. & Sampson, N. S. Cyclic alternating ring-opening metathesis polymerization (CAROMP). Rapid access to functionalized cyclic polymers. *Org. Lett.* **12**, 3729-3731 (2010).

28. Hlil, A. R. et al. Ring opening metathesis polymerization (ROMP) of five-to eight-membered cyclic olefins: Computational, thermodynamic, and experimental approach. *J. Polym. Sci. A Polym. Chem.* **55**, 3137-3145 (2017).

29. Bhaumik, A., Peterson, G. I., Kang, C. & Choi, T. L. Controlled living cascade polymerization to make fully degradable sugar-based polymers from d-glucose and d-galactose. *J. Am. Chem. Soc.* **141**, 12207-12211 (2019).

30. Chen, H., Shi, Z., Hsu, T.-G. & Wang, J. Overcoming the low driving force in forming depolymerizable polymers through monomer isomerization. *Angew. Chem. Int. Ed.* **60**, 25493-25498 (2021).

31. Neary, W. J. & Kennemur, J. G. Polypentenamer renaissance: challenges and opportunities. *ACS Macro Lett.* **8**, 46-56 (2019).

32. Hejl, A., Scherman, O. A. & Grubbs, R. H. Ring-opening metathesis polymerization of functionalized low-strain monomers with ruthenium-based catalysts. *Macromolecules* **38**, 7214–7218 (2005).

33. Dragojlovic, V. Conformational analysis of cycloalkanes. *ChemTexts* **1**, 14 (2015).

34. Bousselat, A., Rouden, J. & Blanchet, J. From building blocks to catalysts: The underinvestigated potential of boronic acid esters. *J. Org. Chem.* **89**, 11009-11013 (2024).

35. Manhas, S. & Taylor, M. S. Dehydrative glycosidations of 2-deoxysugar derivatives catalyzed by an arylboronic ester. *Carbohydr. Res.* **470**, 42-49 (2018).

36. Rodrigues Silva, D., de Azevedo Santos, L., M, P. F., Fonseca Guerra, C. & Hamlin, T. A. Nature and strength of lewis acid/base interaction in boron and nitrogen trihalides. *Chem. Asian. J.* **15**, 4043-4054 (2020).

37. Daintion, F. S., Devlin, T. R. E. & Small, P. A. The thermodynamics of polymerization of cyclic compounds by ring opening. *Trans. Faraday Soc.* **51**, 1710-1720 (1955).

38. Nieboer, V., Wohlert, J., Olsen, P. & Odelius, K. More than ring-strain: revisiting the definition of enthalpy in ring-opening polymerization. *Faraday Discuss* **262**, 311-326 (2026)

39. Kwon, H. & Mpourmpakis, G. Ab initio thermochemistry of highly flexible molecules for thermal decomposition analysis. *J. Chem. Theory. Comput.* **19**, 3652-3663 (2023).

40. Ibrahim, T., Martindale, J., Ritacco, A., Rodriguez, M. & Sun, H. Polyheptenamer: A chemically recyclable polyolefin enabled by the low strain of seven‐membered cycloheptene. *J. Polym. Sci.* **62**, 4921-4927 (2024).

Acknowledgements

This paper is dedicated to Professor Chulbom Lee on the occasion of his 60th birthday. This work was supported by the National Research Foundation of Korea (RS-2023-00277926; NRF-2019R1A6A1A10073887, S. H. H.) and the Korea Research Institute of Chemical Technology (Basic project, S. H. H.) funded by the Korean Government.

Author Contributions

K.C. performed DFT calculations of monomer structures and ERSEs and analyzed their structure–property relationships. K.C., W.C., and M.C. carried out monomer synthesis, polymerization, and polymer characterization. K.C. and B.I. conducted thermomechanical analyses of polymers. S.H.H. conceived and supervised the project. All authors contributed to writing and revising the manuscript.

Competing interests

The authors declare no competing interests.

Tables

Table 1. RCMD results for polymers derived from fused-ring cyclohexene monomers.[a]

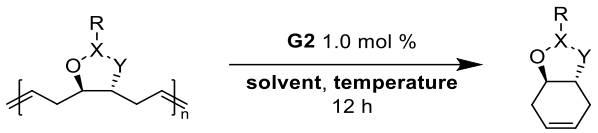

Polymer	T_c (1.0 M)	Conditions	Conversion
PTiPrCbm	0.3 °C[b]	CH_2Cl_2 [0.20 M], 40 °C	>96%
PTPhCbm	61.9 °C	CH_2Cl_2 [0.20 M], 40 °C	94%±0.699
PTtBuCbm	65.9 °C	CH_2Cl_2 [0.20 M], 40 °C	91%±0.241
PTAcCbm	118.2 °C	CH_2Cl_2 [0.10 M], 40 °C	93%±0.394
PTnPrAc	40.7 °C	CH_2Cl_2 [0.30 M], 40 °C	>96%
PTPhAc	30.3 °C	CH_2Cl_2 [0.30 M], 40 °C	93%±1.12
PTCbo	216.2 °C	THF/DMF (2:1) [0.10 M], 40 °C	32%±0.899
PTCbo	216.2 °C	THF/DMF (2:1) [0.10 M], 60 °C	60%±0.486
PTnBuBor	522.5 °C	CH_2Cl_2 [0.10 M], 40 °C	46%±1.12
PTPhBor	240.9 °C	CH_2Cl_2 [0.10 M], 40 °C	51%±0.649
PTnBuBor	522.5 °C	THF [0.10 M], 60 °C	48%±0.982
PTPhBor	240.9 °C	THF [0.10 M], 60 °C	51%±1.40
PC6diol	-	THF/DMF (2:1) [0.32 M], 25 °C	>96%

[a] All results were averaged over 3 independent experiments, errors denote standard deviation. The conversion was measured via comparison of olefin peaks in ^{1}H NMR spectra. [b] T_c value was calculated from 2.0 M condition due to the monomer reactivity.

Figure Legends/captions

Figure 1. Reversible ROMP of cyclohexene monomers (C6-ROMP). This figure contrasts historical limitations in cyclohexene ROMP with the C6-ROMP design concept based on fused five-membered heterocycles. The library of monomers prepared in this study is shown together with their DFT-calculated ERSEs.

Figure 2. Conformational effect in trans- and cis- heterocycle fused cyclohexene monomers. The diagrams illustrate how the geometric mismatch in trans-fused monomers generates ring strain through conformational distortion, whereas cis-fused isomers suffer from steric repulsion upon ring opening that lowers their overall strain energy.

Figure 3. ERSEs and optimized structures of acetal and silyl ether monomers. DFT-calculated structures and ERSE values are shown for acetal and silyl ether monomers, demonstrating that trans-fused acetals exhibit sufficient conformational strain for polymerization, while flexible silyl ethers and cis-fused variants show lower stain and no polymerizability under the tested conditions.

Figure 4. ERSEs and calculated structures of carbonate, carbamate, and boronic ester monomers. DFT-optimized cyclic and ring-opened structures with ERSEs are presented for carbonate, carbamate, and boronic ester monomers. The figure emphasizes the roles of fusion stereochemistry, substituent sterics, and heterocycle flexibility in governing ring-strain modulation across these classes.

Figure 5. Substituent effects in carbamate monomers. Steric effects of the N-substituents are quantified by the change in the substituent–allylic carbon distance ($d-d'$) between the cyclic and ring-opened structures.

Figure 6. Polymerization thermodynamic parameters for C6-ROMP of fused-ring cyclohexene monomers. Experimentally determined polymerization enthalpies (ΔH_p) and entropies (ΔS_p), together with the calculated ceiling temperatures (T_c), are summarized for polymerizable monomers. The data establish structure–thermodynamics relationships that govern polymerization feasibility under the tested conditions. [a]Obtained from 2.0 M initial concentration. [b]Obtained from 1.0 M initial concentration.

Figure 7. Polymerization entropy (ΔS_p) for fused-ring cyclohexene monomers. Experimental ΔS_p values are compared for polymerizable monomers measured at initial monomer concentrations of 1.0 M and 2.0 M in CH_2Cl_2. The concentration dependence highlights how substituents and intermolecular interactions modulate the entropic term of polymerization.

Figure 8. ERSE–thermodynamics relationships and concentration effects. a. Correlation between ERSE and ΔH_p at 2.0 M. **b.** Correlation between ERSE and ΔH_p at 1.0 M. **c.** Concentration dependence of ΔH_p and ΔS_p for **TPhAc**. **d.** Concentration dependence of ΔH_p and ΔS_p for **TnPrAc**.

Figure 9. Polymer properties for selected C6-ROMP polymers. Number-average molecular weight (M_n), dispersity (Đ), glass transition temperature (T_g), and decomposition temperature (T_d) are reported for polymers prepared at a monomer-to-initiator ratio of 1000:1 in CH_2Cl_2 (2.0 M).

Editorial Summary:
Performing ring opening metathesis polymerisation of cyclohexene is challenging due to its low ring strain. Here, cyclohexene-derived monomers were designed with varying ring strains to tailor their polymerisation and depolymerisation thermodynamics, providing a guideline for future monomer design.

Peer review information: Nature Communications thanks the anonymous reviewers for their contribution to the peer review of this work. A peer review file is available.

McCarthy 1986

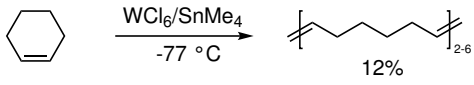

Chen 2022

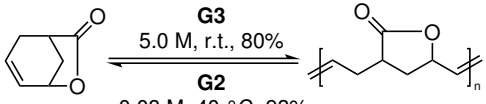

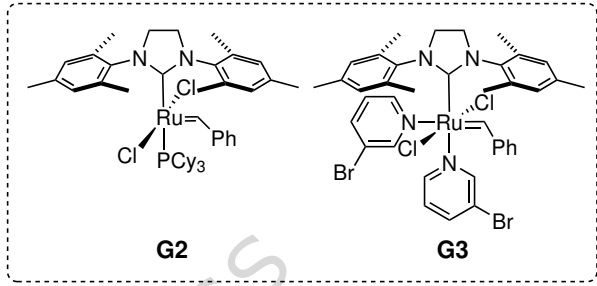

This work:

Reversible ROMP of Cyclohexene Derivatives via Adaptive Ring Strain Modulation

ERSE

- DFT based evaluation
- Prediction of reactivity

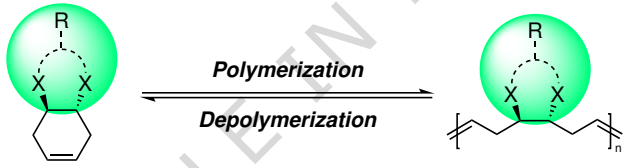

?H_p ?S_p

- Experimental data
- Substituent effects

ERSE (kcal/mol):

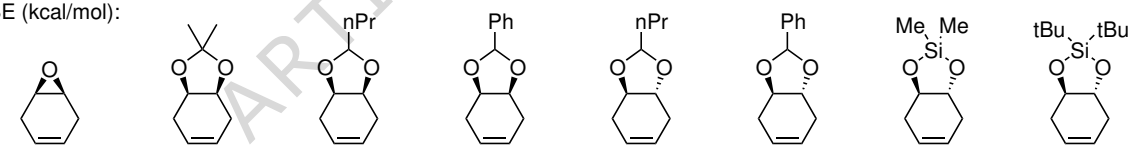

45EP	**CdiMeAc**	**CnPrAc**	**CPhAc**	**TnPrAc**	**TPhAc**	**TdiMeSil**	**TditBuSil**
-0.65	1.94	1.81	1.15	4.44	4.30	2.56	2.78

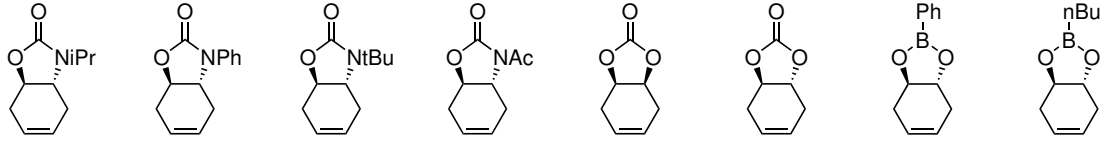

TiPrCbm	**TPhCbm**	**TtBuCbm**	**TAcCbm**	**CCbo**	**TCbo**	**TPhBor**	**TnBuBor**
4.25	5.10	5.25	5.54	0.91	6.00	6.04	6.22

- Unlocking the potential of cyclohexene derivatives: C_6-ROMP
- Thermodynamic control for predictable polymerization and efficient recyclability
- Structure-reactivity relationship for designing chemically recyclable and functional polymers

Free heterocycles:

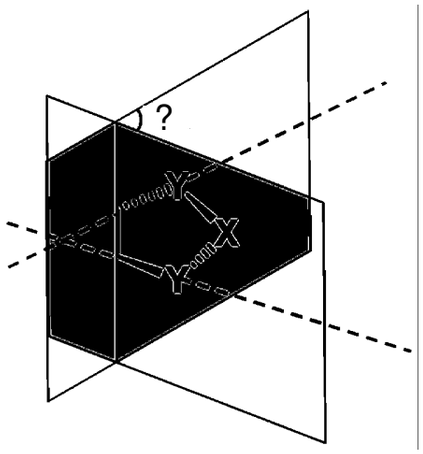

?: dihedral anlge between Y–C–C–Y

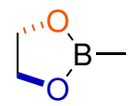
? = 0.02°

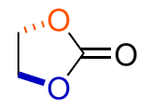
? = 22.6°

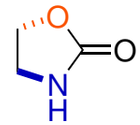
? = 26.3°

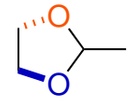
? = 26.4°

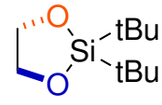
? = 30.8°

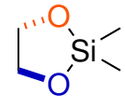
? = 34.3°

Heterocycle conformations:

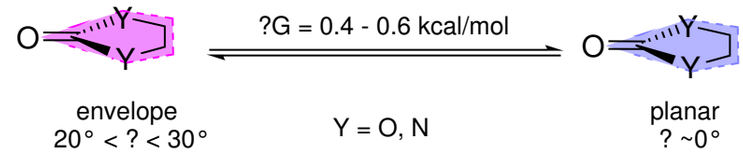

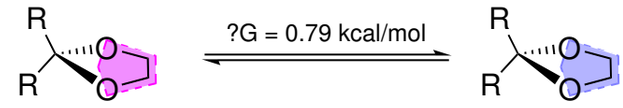

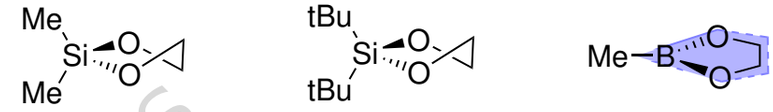

Trans-fused:

Cyclic form

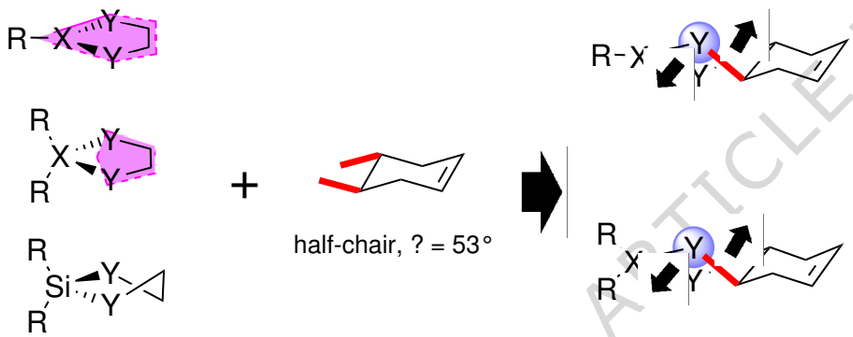

X = B, C (? < 30°)
X = Si (? > 30°)
Y = O, N

strained conformations

Ring-opened form

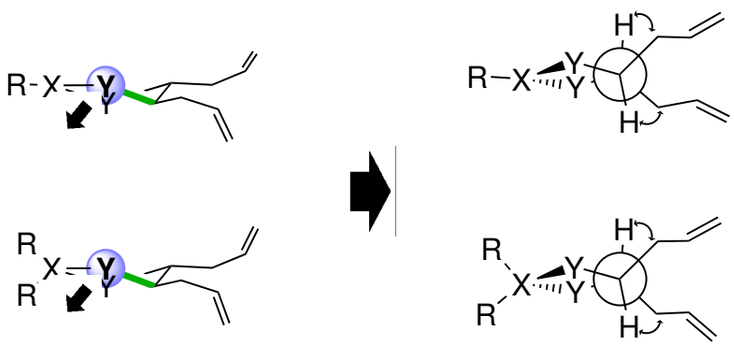

increased rotational freedom

decreased C–Y dihedral angle

less sterically hindered

Cis-fused:

Cyclic form

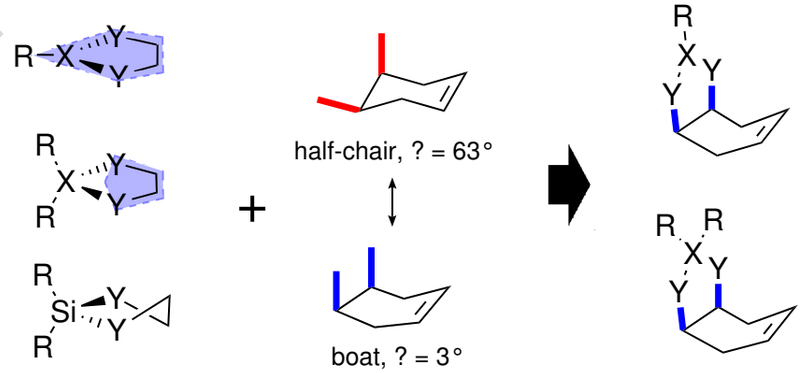

X = B, C (? ~0°)
X = Si (? > 30°)
Y = O, N

well aligned conformations

Ring-opened form

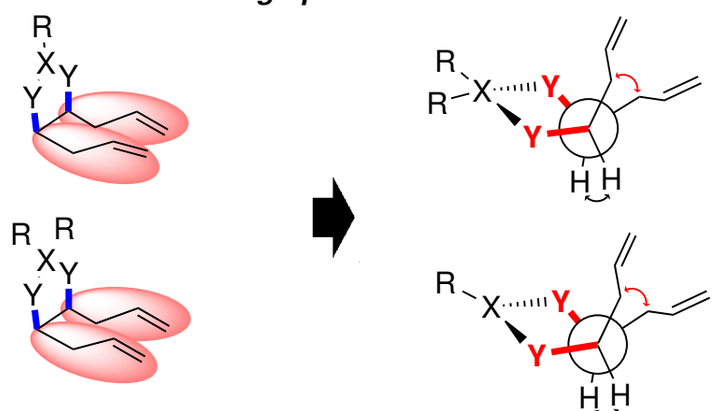

increased steric hindrance (eclipsing alkyl chain)

increased C–Y dihedral angle

more sterically hindered

Cis-fused monomers

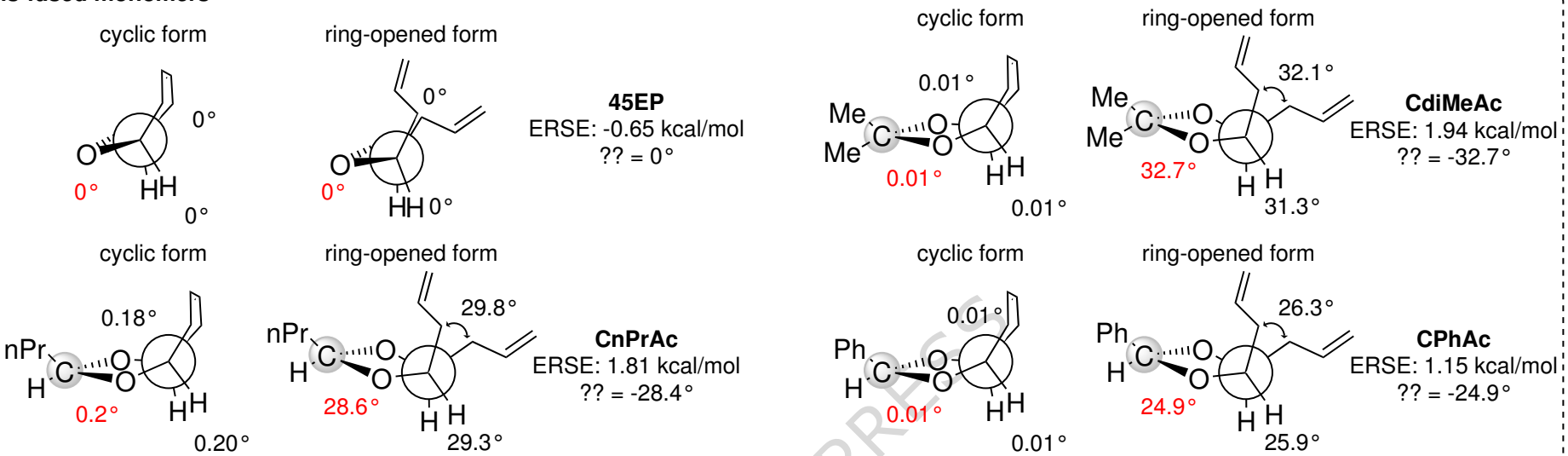

Trans-acetal monomers

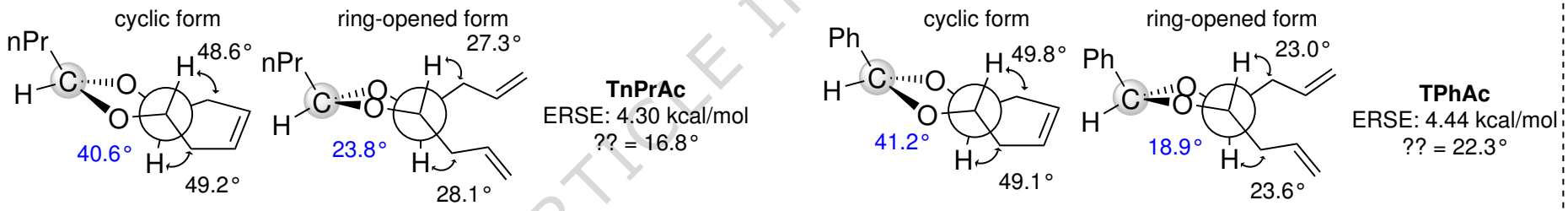

Silyl ether monomers

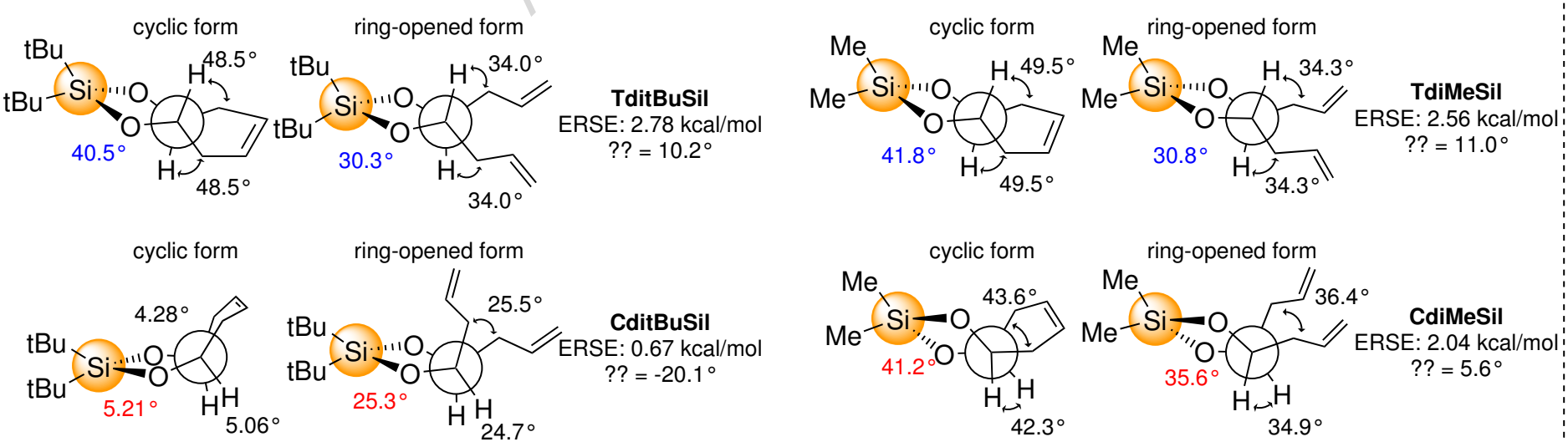

Carbonate (sp^2) monomers

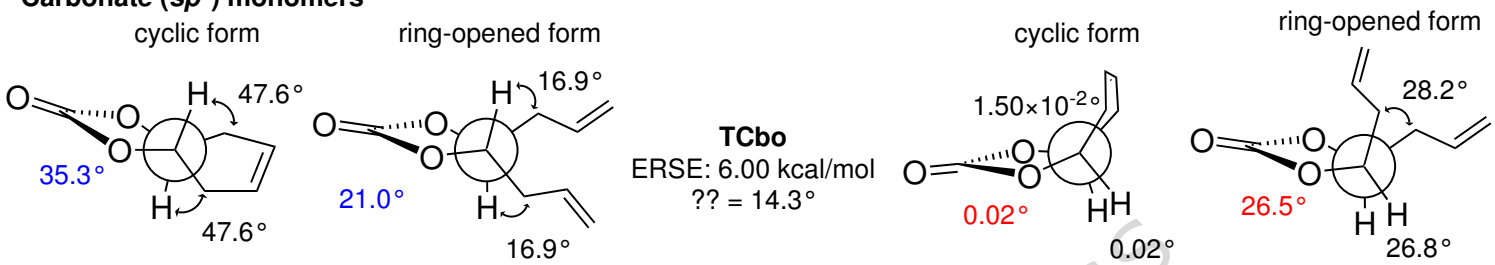

TCbo
ERSE: 6.00 kcal/mol
?? = 14.3°

CCbo
ERSE: 0.91 kcal/mol
?? = -26.5°

Carbamate (sp^2) monomers

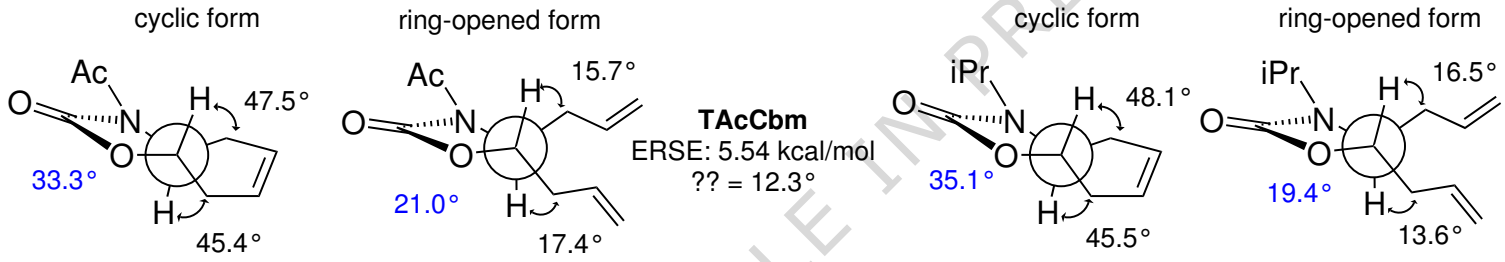

TAcCbm
ERSE: 5.54 kcal/mol
?? = 12.3°

TiPrCbm
ERSE: 4.25 kcal/mol
?? = 15.7°

TPhCbm
ERSE: 5.10 kcal/mol
?? = 11.2°

TtBuCbm
ERSE: 5.25 kcal/mol
?? = 6.6°

Boronic ester (sp^2-empty p) monomers

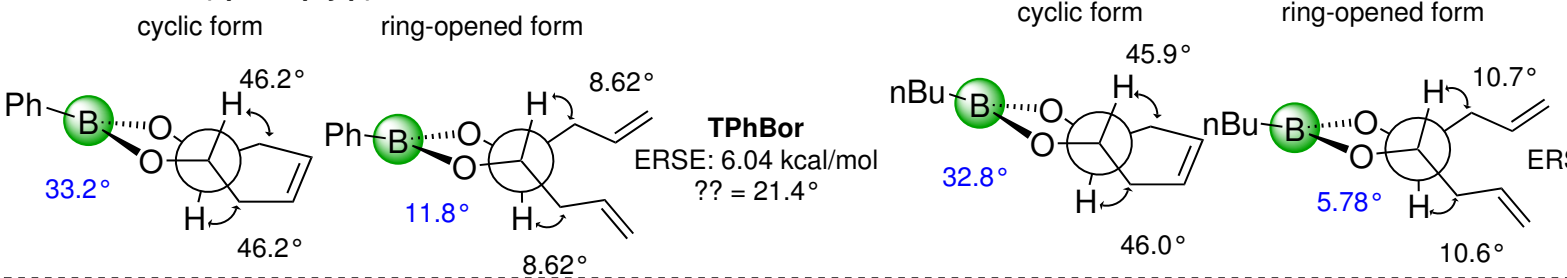

TPhBor
ERSE: 6.04 kcal/mol
?? = 21.4°

TnBuBor
ERSE: 6.22 kcal/mol
?? = 27.0°

TiPrCbm

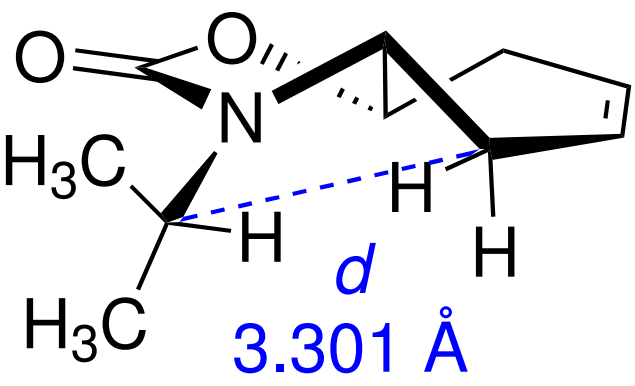

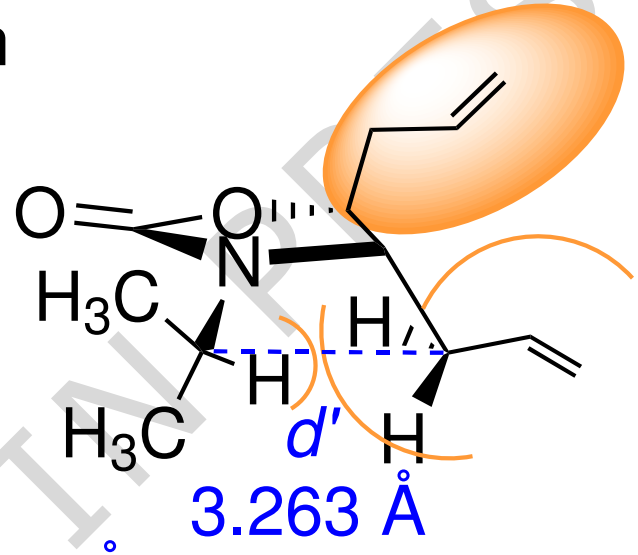

d-*d*′ = –0.038 Å

TtBuCbm

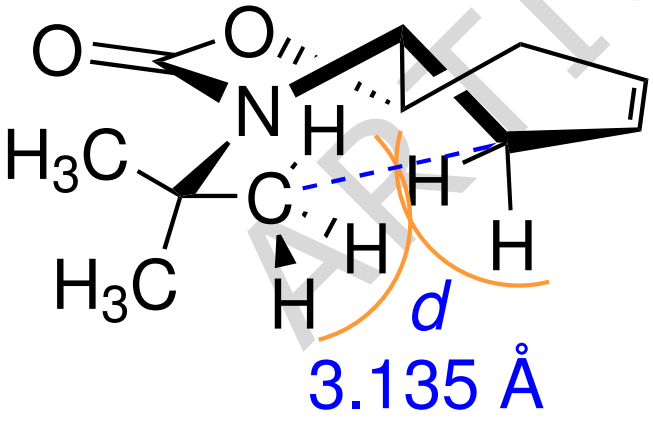

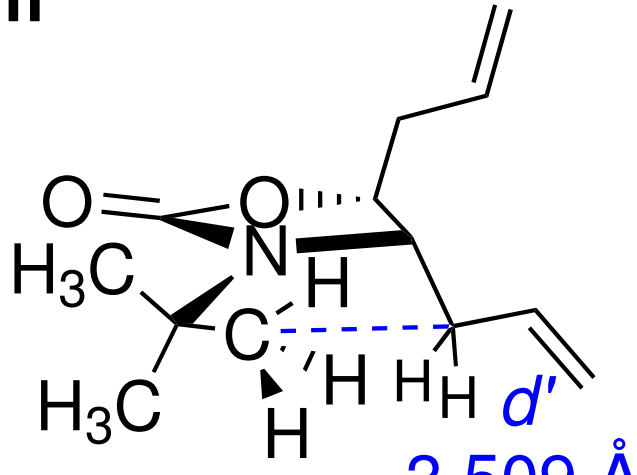

d-*d*′ = 0.374 Å

45EP
ERSE: -0.65 kcal/mol
not polymerizable

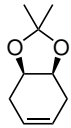

CdiMeAc
ERSE: 1.94 kcal/mol
not polymerizable

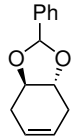

TPhAc
ERSE: 4.30 kcal/mol
?H_p: -3.52 kcal/mol[a]
?S_p: -12.4 cal/mol·K[a]
T_c: 30.3 °C[b]

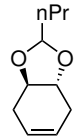

TnPrAc
ERSE: 4.44 kcal/mol
?H_p: -2.08 kcal/mol[a]
?S_p: -7.65 cal/mol·K[a]
T_c: 40.7 °C[b]

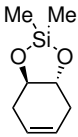

TdiMeSil
ERSE: 2.56 kcal/mol
not polymerizable

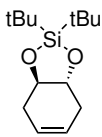

TditBuSil
ERSE: 2.78 kcal/mol
not polymerizable

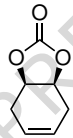

CCbo
ERSE: 0.91 kcal/mol
not polymerizable

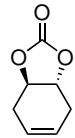

TCbo
ERSE: 6.00 kcal/mol
?H_p: -3.92 kcal/mol[a]
?S_p: -7.99 cal/mol·K[a]
T_c: 216.2 °C[b]

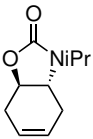

TiPrCbm
ERSE: 4.25 kcal/mol
?H_p: -1.85 kcal/mol[a]
?S_p: -6.77 cal/mol·K[a]
T_c: 0.335 °C[a]

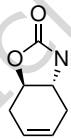

TPhCbm
ERSE: 5.10 kcal/mol
?H_p:-2.64 kcal/mol[a]
?S_p: -7.90 cal/mol·K[a]
T_c: 61.9 °C[b]

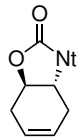

TtBuCbm
ERSE: 5.25 kcal/mol
?H_p: -3.73 kcal/mol[a]
?S_p: -11.3 cal/mol·K[a]
T_c: 65.9 °C[b]

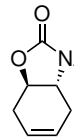

TAcCbm
ERSE: 5.54 kcal/mol
?H_p: -3.25 kcal/mol[a]
?S_p: -8.68 cal/mol·K[a]
T_c: 118.2 °C[b]

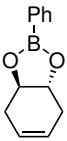

TPhBor
ERSE: 6.04 kcal/mol
?H_p: -2.62 kcal/mol[a]
?S_p: -5.48 cal/mol·K[a]
T_c: 240.9 °C[b]

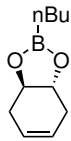

TnBuBor
ERSE: 6.22 kcal/mol
?H_p: -1.59 kcal/mol[a]
?S_p: -1.21 cal/mol·K[a]
T_c: 522.5 °C[b]

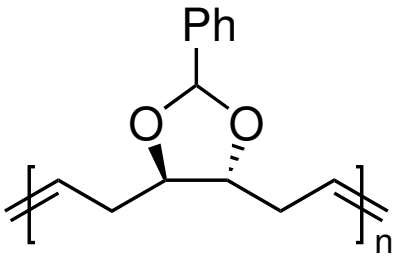

PTPhAc
M_n: 46.1 kDa, Đ: 1.54
T_g: 24 °C, T_d: 130 °C

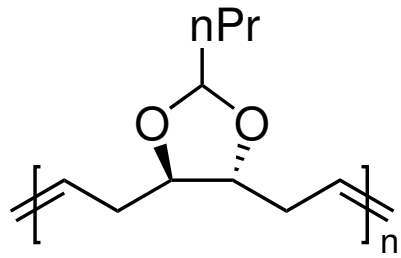

PTnPrAc
M_n: 13.2 kDa, Đ: 1.59
T_g: -29 °C, T_d: 231 °C

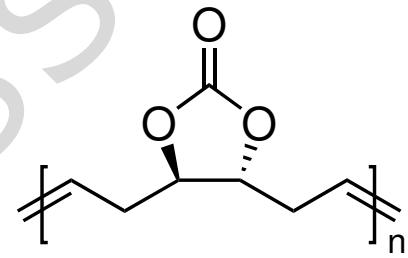

PTCbo
M_n: 146 kDa, Đ: 1.19
T_g: 65 °C, T_d: 314 °C

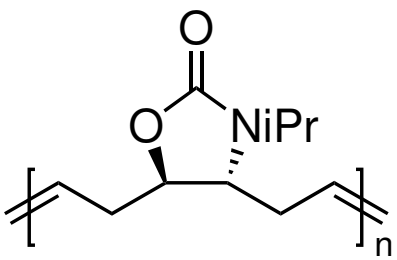

PTiPrCbm
M_n: 34.8 kDa, Đ: 1.15
T_g: 70 °C, T_d: 286 °C

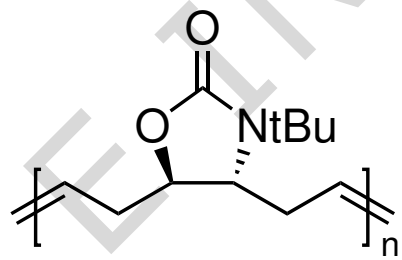

PTtBuCbm
M_n: 86.1 kDa, Đ: 1.37
T_g: 120 °C, T_d: 356 °C

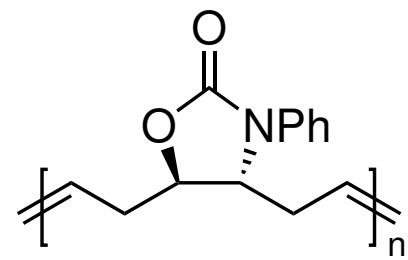

PTPhCbm
M_n: 99.7 kDa, Đ: 1.50
T_g: 73 °C, T_d: 274 °C

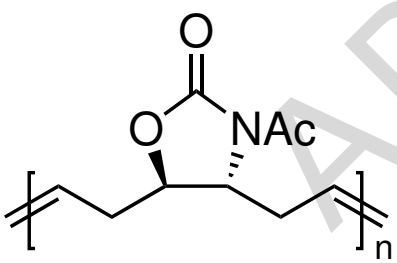

PTAcCbm
M_n: 99.2 kDa, Đ: 1.35
T_g: 82 °C, T_d: 221 °C

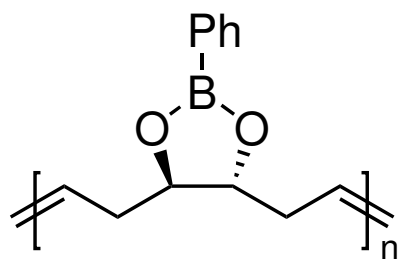

PTPhBor
M_n: 74.6 kDa, Đ: 1.85
T_g: 52 °C, T_d: 268 °C

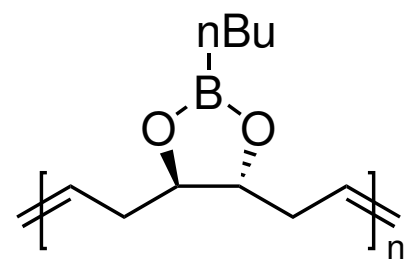

PTnBuBor
M_n: 44.1 kDa, Đ: 2.00
T_g: -42 °C, T_d: 265 °C

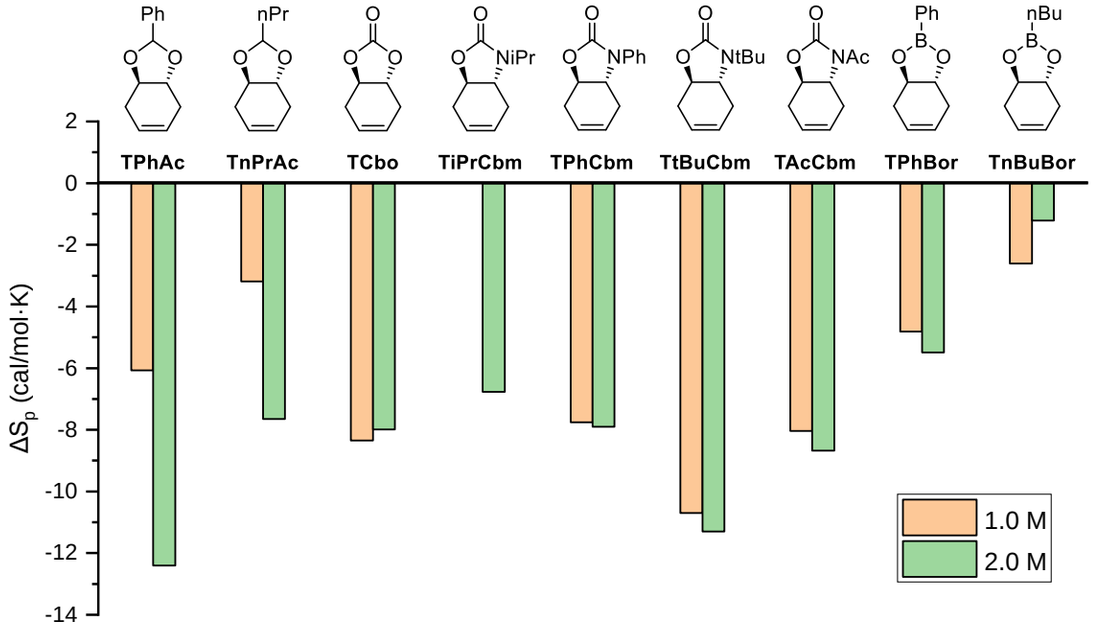
Ph
nPr
O
NiPr
NPh
NtBu
NAc
Ph
B
nBu
B
TPhAc
TnPrAc
TCbo
TiPrCbm
TPhCbm
TtBuCbm
TAcCbm
TPhBor
TnBuBor
2
0
-2
-4
-6
-8
-10
-12
-14
ΔSp (cal/mol·K)
1.0 M
2.0 M

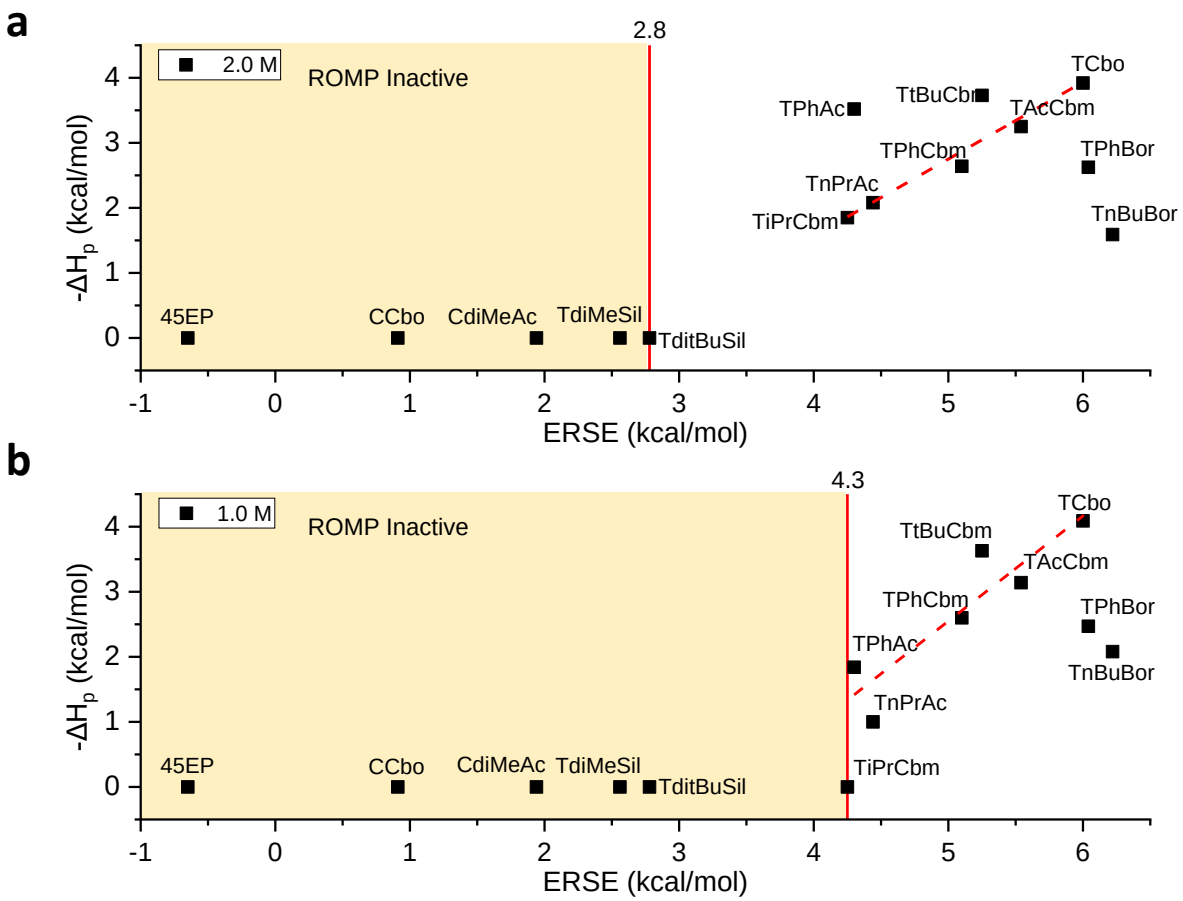
a
2.0 M
ROMP Inactive
2.8
-ΔHp (kcal/mol)
ERSE (kcal/mol)
45EP
CCbo
CdiMeAc
TdiMeSil
TditBuSil
TPhAc
TtBuCbm
TCbo
TAcCbm
TPhCbm
TPhBor
TnPrAc
TiPrCbm
TnBuBor

b
1.0 M
ROMP Inactive
4.3
-ΔHp (kcal/mol)
ERSE (kcal/mol)
45EP
CCbo
CdiMeAc
TdiMeSil
TditBuSil
TCbo
TtBuCbm
TAcCbm
TPhCbm
TPhBor
TPhAc
TnBuBor
TnPrAc
TiPrCbm

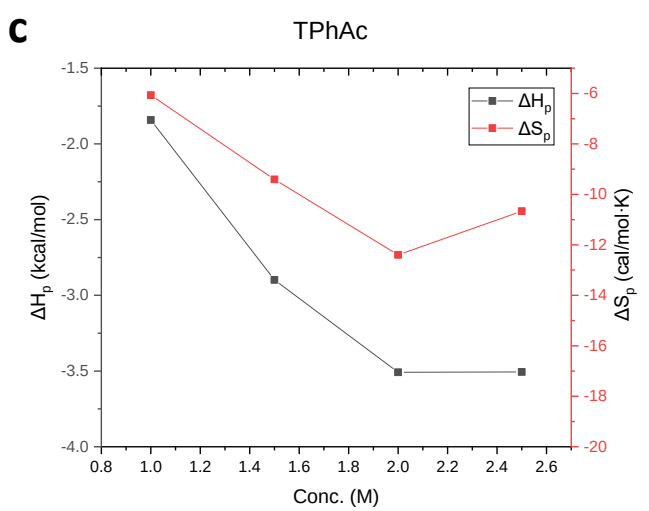
c
TPhAc
ΔHp
ΔSp
ΔHp (kcal/mol)
ΔSp (cal/mol·K)
Conc. (M)

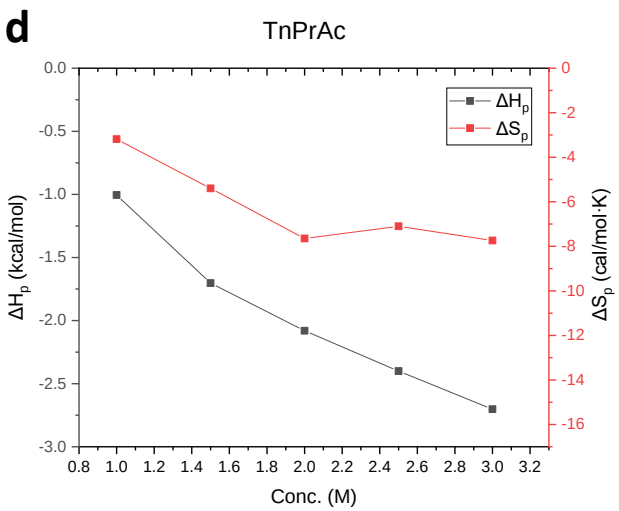
d
TnPrAc
ΔHp
ΔSp
ΔHp (kcal/mol)
ΔSp (cal/mol·K)
Conc. (M)